



HAL
open science

New Architecture Based on Metal-Organic Frameworks and Spin Crossover Complexes to Detect Volatile Organic Compounds

Emmelyne Cuza, Gilles Patriarche, Christian Serre, Antoine Tissot

► **To cite this version:**

Emmelyne Cuza, Gilles Patriarche, Christian Serre, Antoine Tissot. New Architecture Based on Metal-Organic Frameworks and Spin Crossover Complexes to Detect Volatile Organic Compounds. *Chemistry - A European Journal*, 2024, 30 (38), pp.e202400463. 10.1002/chem.202400463 . hal-04787690

HAL Id: hal-04787690

<https://hal.science/hal-04787690v1>

Submitted on 17 Nov 2024

HAL is a multi-disciplinary open access archive for the deposit and dissemination of scientific research documents, whether they are published or not. The documents may come from teaching and research institutions in France or abroad, or from public or private research centers.

L'archive ouverte pluridisciplinaire **HAL**, est destinée au dépôt et à la diffusion de documents scientifiques de niveau recherche, publiés ou non, émanant des établissements d'enseignement et de recherche français ou étrangers, des laboratoires publics ou privés.



Distributed under a Creative Commons Attribution 4.0 International License

New Architecture Based on Metal-Organic Frameworks and Spin Crossover Complexes to Detect Volatile Organic Compounds

Emmelyne Cuza,^[a] Gilles Patriarche,^[b] Christian Serre,^{*,[a]} and Antoine Tissot^{†,*[a]}

We present here the encapsulation of a spin crossover complex C^1 [Fe^{II}(L)] (L: 4-amino-, 2-(2-pyridinylmethylene)hydrazide) inside MOF-808(Zr), a chemically robust Metal-Organic Framework. The compound C^1 MOF-808 retains its crystallinity as well as a partial porosity compared to pristine MOF and shows solvatochromism under Volatile Organic compounds (VOCs)

sorption associated to a spin state change of the guest complex. More specifically, this compound shows an interesting reversible color change under formaldehyde and formic acid vapor sorption and can therefore be considered as a new kind of optical VOCs chemosensor, opening new doors for developing a broad range of VOCs optical sensors.

1. Introduction

In the recent years, a new worldwide concern has appeared about indoor air quality^[1] and more specifically about volatile organic compounds (VOCs). The European Union as well as the World Health Organization defined them as organic compounds having at room temperature a vapor pressure higher than 0.01 kPa, and/or any moieties with a corresponding volatility under other particular condition.^[2] A majority of them, in particular aromatic compounds, unsaturated and saturated hydrocarbons or small organic molecules showed a highly damaging impact on the health.^[3] Those side-effects range from mild irritation to heavy symptoms such as the appearance of serious chronic illnesses to even cancers and are directly linked to the concentration and time of exposure. European Union as well as OSHA (Occupational Safety and Health Administration U.S.A.), defined some compounds as more hazardous than others like formaldehyde, styrene derivatives or toluene. The accurate identification and quantification of those compounds can be done using costly equipment, such as mass spectrometry.^[4] In practice, other types of instruments like photo-ionization detectors or one-use colorimetric detectors are quite commonly used, but these kinds of detectors come with some problem, like their non-selectivity and cross-contamination (for one

specific pollutant, the presence of other VOCs can compromise the measured value).

One strategy to overcome these drawbacks is to design specific switchable compounds that would interact with targeted VOCs only. These compounds should show a reversible switching and be reusable once taken out of the VOCs environment, as well as being stable and robust with time. For that, one approach is to rely on bistable materials such as spin crossover compounds (SCO) that can switch from one electronically stable state to another (*High Spin* (HS) ↔ *Low Spin* (LS)). These compounds are highly sensitive to their environment,^[5] since their switching properties can be triggered by physical (temperature, pressure, light irradiation, magnetic or electric field)^[6] or chemical (solvent, counter-ion, ligand)^[7] external stimuli. The SCO phenomenon is accompanied by changes of many physical properties (magnetic susceptibility, color, elastic properties, thermal/electric conductivity etc.) making these compounds suitable candidates for sensing applications. For example, Kitagawa and al.^[8] presented in 2009 a Hoffmann clathrate,^[9] [Fe(pyrazine)Pt(CN)₄] with a particular affinity associated to a spin state change upon CS₂ or benzene vapor sorption while still being sensitive to other gases. However, most SCO compounds are not porous and/or non-selective and/or in most cases are poorly chemically stable, for example under humid conditions. One way to overcome these drawbacks is to use a vessel to protect the complex. Such a carrier needs to be physically and chemically robust, diamagnetic, colorless and must let VOCs interact with the SCO complex.

Water stable Metal-organic Frameworks (MOFs) are promising materials to host spin crossover complexes. MOFs are 3D-self assembled porous solids composed of organic ligands and inorganic sub-units (metal ions or oxo-clusters, chains, layers...) that presents a large panel of structures with highly organized meso- or microporous channels or cages.^[10] Their self-assemblies' properties can lead to tunable architectures through various post-synthetic methods. Such compounds have been extensively studied for the past two decades years for their remarkable properties,^[11] and their numerous possible applica-

[a] E. Cuza, C. Serre, A. Tissot
Institut des Matériaux Poreux de Paris, Ecole Normale Supérieure, ESPCI
Paris, CNRS, PSL University, 75005 Paris, France
E-mail: christian.serre@ens.psl.eu
antoine.tissot@ens.psl.eu

[b] G. Patriarche
Centre de Nanosciences et de Nanotechnologies, Université Paris-Saclay,
CNRS, 91120, Palaiseau, France

Supporting information for this article is available on the WWW under
<https://doi.org/10.1002/chem.202400463>

© 2024 The Authors. Chemistry - A European Journal published by Wiley-VCH GmbH. This is an open access article under the terms of the Creative Commons Attribution License, which permits use, distribution and reproduction in any medium, provided the original work is properly cited.

tions, from separation, catalysis, bio-application to molecular capture and sensing, among others.^[12] Even if by themselves, MOFs are good candidates for sensing applications,^[13] the vast majority of them does not exhibit any switching properties and the rare one that can be used for detection are often luminescent compounds that requires a light excitation, which is less practicable than having colorimetric switch in the visible.^[14] By adding a SCO complex inside the pores of the MOF, these drawbacks could be overcome, since in that case, the MOF could be engineered to capture targeted analytes while the sensing part would come from the bistable nature of SCO entity.

One of the first example of the loading of SCO complexes inside MOFs was published in 2016 by Zhao et al.^[15], where one successfully loaded $[\text{Fe}^{\text{II}}(\text{HB}(\text{pz})_3)_2]$ into the mesoporous NH_2 -MIL-101(Al) through the bottle-around-the-ship strategy. This porous solid showed a change of spin state when put directly in contact with different solvents. More recently, Moreau et al. reported the anchoring of $[\text{Fe}^{\text{II}}(\text{BPI})(\text{HBPI})(\text{ClO}_4)_2]^-$ complexes in MFU-4l and MIL-100(Al), leading to porous materials exhibiting a solvatochromic switching upon sorption of alcohols in suspension.^[16] However, in both cases, no optical measurements were performed in presence of vapors.

In 2019, some of us reported the encapsulation via a ship-in-the-bottle strategy of the $[\text{Fe}^{\text{III}}(\text{sal}_2\text{trien})]^+$ SCO complex inside the mesoporous MIL-100(Al). This hybrid compound showed a remarkable reversible SCO switch upon sorption of water vapors,^[17] evidencing for the first time that these hybrid compounds can be used as optical sensor of vapors. More recently, Shen et al.^[18] reported the encapsulation of the same SCO complex inside MOF-808(Zr) leading to a compound presenting a thermal spin state switching around room temperature with the opening of a large hysteresis loop, suggesting again the potential of SCO-MOF hybrid solids for sensing applications.

As a benchmark MOF material,^[19–20] MOF-808(Zr) or $\text{Zr}_6\text{O}_4(\text{OH})_4(\text{C}_6\text{H}_3(\text{CO}_2\text{H})_3)_2(\text{HCOO})_6$ is a Zr(IV)-tricarboxylate built with two types of cages, one narrow ($\phi \sim 4.8 \text{ \AA}$) and a large adamantane cage with a free diameter of 18.4 \AA . Diamagnetic, white and chemically stable, this MOF is a promising candidate to encapsulate SCO complexes and to possibly enhance concentration/capture VOCs vapors around a targeted SCO complex loaded in its large pores. Here, we report the encapsulation in MOF-808(Zr) of an Fe(II) spin crossover complex based on an acylhydrazone ligand described by Chen et al. in 2019^[21]: $\text{Fe}(\text{L}_2)_2 \cdot 2\text{H}_2\text{O}$ (L: 4-amino-2-(2-pyridinylmethylene)-hydrazide) noted C^1 . This neutral mononuclear complex possesses a spin transition around room temperature ($T_{1/2} \approx 320 \text{ K}$) and changes of magnetic properties under the influence of solvent vapors. It is therefore a very good candidate for the design of a sensor due to its intrinsic ability to interact with different solvents and its switchable behavior near room temperature, thereby one of the few complexes that can be used in those conditions. We report in the following the synthesis, characterization and testing of a hybrid C^1 -MOF-808(Zr) film and evidence that this compound can be used for the

colorimetric sensing of formaldehyde and formic acid based on a spin state switching.

2. Results and Discussion

2.1. Synthesis

60 nm-MOF-808 nanocrystals were synthesized as previously described (See ESI*^[20]). The complex $\text{Fe}(\text{L}_2)_2 \cdot 2\text{H}_2\text{O}$ (L: 4-amino-2-(2-pyridinylmethylene)-hydrazide), noted after C^1 , was synthesized by a modification of an already published protocol (see ESI*^[21,22]). The hybrid compound was prepared by loading the complex C^1 in a suspension of MOF-808 in acetonitrile (using a 3:1 MOF:complex weight ratio). The mixture was stirred for 12 hours and then washed thoroughly to remove non adsorbed complexes (see ESI*^[20]). The resulting compound is obtained as a kaki green color powder and noted C^1 -MOF-808. The vibrant color (compared to the white MOF-808 powder) obtained after several washing steps (until the solvent is clear at least three times) suggests the successful encapsulation of C^1 through strong host-guest interactions between the two compounds.

2.2. Characterisation and Magnetic Properties

Powder X-Ray Diffraction (PXRD) measurements of C^1 , MOF-808, and C^1 -MOF-808, confirm the preservation of the host structure after loading (Figure 1a). In addition, characteristic Bragg peaks of C^1 are absent in the loaded hybrid material, indicating that no recrystallization of C^1 occurs during the loading process.

The infrared spectrum of C^1 -MOF-808 (Figure 1b) confirms the integrity of the MOF as well as the successful loading of the spin crossover complex in the hybrid compound. Indeed, characteristic vibrational bands $\nu_{\text{NH}_2} = 3329$, $\nu_{\text{N}=\text{C}} = 1602$, $\nu_{\text{CO}^-} = 1360 \text{ cm}^{-1}$ as well as all the aromatic stretching between 1200 – 1100 cm^{-1} , and the deformation band corresponding to the pyridine aromatic mono-substituted around 760 cm^{-1} confirm the presence of the complex C^1 as well as its integrity in C^1 -MOF-808. For MOF-808, some characteristic bands $\nu_{\text{C}=\text{O}}(\text{formate}) = 1624$, $\nu_{\text{C}=\text{O}}(\text{BTC}) = 1597$, $\nu_{\text{O}^-} = 1382$ and $\nu_{\text{C}=\text{C}}(\text{BTC}) = 650 \text{ cm}^{-1}$ are also found in C^1 -MOF-808, evidencing the presence of the two compounds with no alteration in the hybrid material (Table S1*^[20]).

Nitrogen porosimetry experiments have been performed on MOF-808 and C^1 -MOF-808 (Figure S8a). For MOF-808, both BET surface area ($2020 \pm 20 \text{ m}^2/\text{g}$) and nitrogen uptake ($431 \text{ cm}^3/\text{g}$) are in agreement with previously published results.^[19] For C^1 -MOF-808, a decrease of almost 50% is observed on the BET surface area ($1220 \pm 20 \text{ m}^2/\text{g}$) compared to the pristine MOF-808. Moreover, the pore size distributions before and after loading (Figure S8b) indicate a decrease of the average pore size, in agreement with the fact that the pores are partially filled, comforting the idea of a successful loading of C^1 inside the pores of MOF-808. (Table S2) In addition, considering that the volume of C^1 (calculated by using the structure obtained by single crystal x-ray diffraction^[21]) is around 1046 \AA^3 and that the

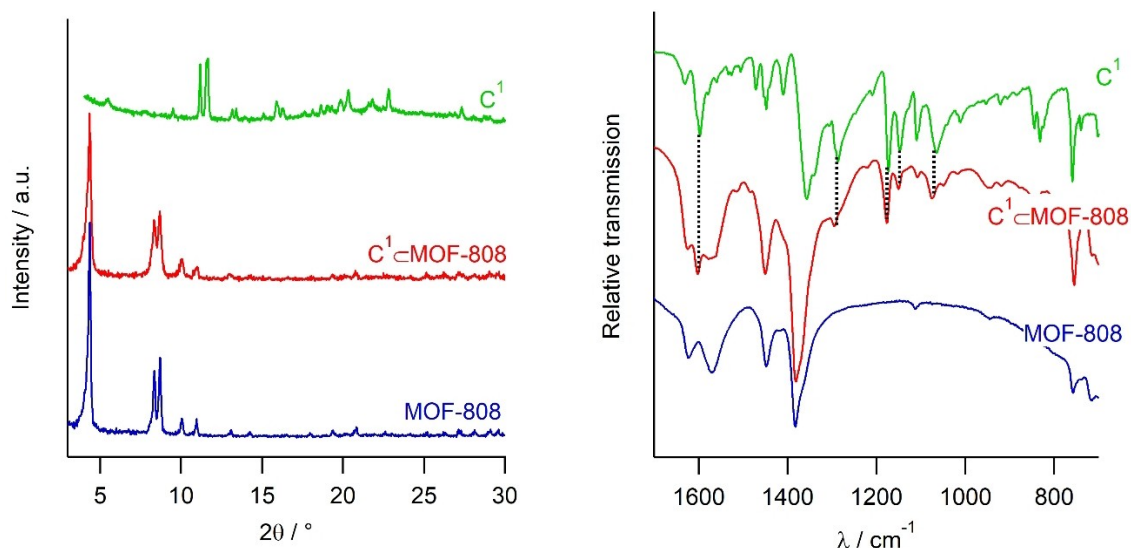


Figure 1. (left) Comparison of PXRD patterns at 298 K ($\lambda_{\text{Cu}} = 1.5418 \text{ \AA}$) of C^1 (green), MOF-808 (blue), $\text{C}^1\text{@MOF-808}$ (red); (right) Comparison of Infrared spectra at 298 K of C^1 , MOF-808 and $\text{C}^1\text{@MOF-808}$ (same color code as Figure 1a).

volume of a single large cage of MOF-808 is around 5400 \AA^3 (assuming a spherical cage with a diameter of 18.4 \AA , not counting the 4.8 \AA tetrahedral cages as they are too small to accommodate a complex), the theoretical maximum number of complexes/cages is estimated at 5.1 C^1/cage .

STEM images (Figure 2, Figure S10) show that the crystal size and shape doesn't change after loading, which confirms the MOF integrity. In addition, SEM images (Figure S9) coupled with Energy dispersive X-ray spectroscopy (EDX) (Table S3) evidence that Fe is homogeneously dispersed inside the MOF crystals (atomic Zr/Fe ratio of 81/19). The homogeneity of the loading at the single particle scale was further observed with

STEM-EDX mapping (Figure 2, Table S4), with an atomic Zr/Fe ratio of 82.4/17.6 corresponding to a ratio of 4.6 complexes/pores, in good agreement with N_2 sorption isotherms as well as with TGA (See ESI* Figure S11, Table S5).

Then the magnetic properties of the hybrid compound were studied and compared to the pristine complex C^1 (Figure S12). Once encapsulated, C^1 doesn't show any thermal SCO behavior and the compound remains in an intermediate state whatever the temperature (50% HS and 50% LS, $\chi_M T$ around $1.8 \text{ cm}^3 \text{ mol K}^{-1}$). The fact that we lost the thermal SCO properties of C^1 may be due to the disappearance of the intermolecular interactions present inside the lattice of C^1

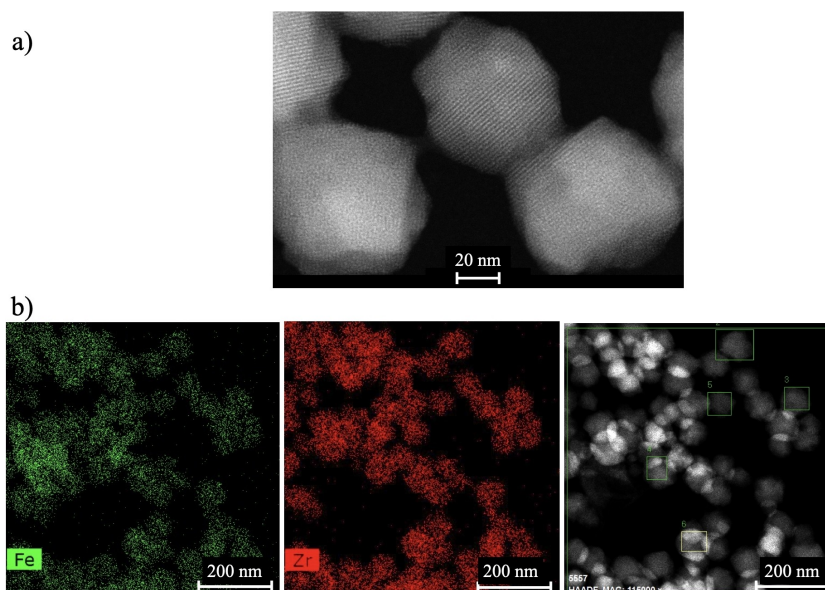


Figure 2. a) Atomic resolution HAADF STEM image of hybrid material nanocrystals of $\text{C}^1\text{@MOF-808}$; b) STEM-EDX elemental mapping map 1 of $\text{C}^1\text{@MOF-808}$ 60 nm nanocrystals.

crystals. Nevertheless, the possibility of the VOCs interacting with the complex is still pending and might lead to a switch to the LS or the HS state.

2.3. VOCs Sensing Studies

2.3.1. UV-Visible Absorption Studies in Liquid Phase of the Ligand and the Complex C^1

Before studying the C^1 MOF-808 hybrid compound, UV-visible studies in solution were carried out to test which solvent can impact the spin state of C^1 . Based on the published results,^[21] a panel of solvent was tested, evidencing the solvatochromic behavior of this complex (Figure 3a). In most cases, two MLCT absorption bands are observed with an isosbestic point at 359 nm due to a solvent-dependent equilibrium between two spin states. On the opposite, HCl modifies the general allure of the spectrum (not the same isosbestic point as others), implying other phenomena than solvent-induced SCO behavior (See ESI Figure S13).

To confirm that the differences observed in most solvents (except HCl) are due to a difference of spin state, we studied the optical spectra of a solution of C^1 in DMF at variable temperature (Figure S14a-b). As observed, the absorbance band at 402 nm disappears to the expense of a band around 323 nm when the solution is heated up. This phenomenon is reversible when cooling down the solution, as expected for a thermally induced spin crossover. On the opposite, as previously

described, the changes observed in presence of HCl are due to a modification of the coordination environment.^[3] More precisely, the HS to LS switch was attributed to a de-coordination, protonation and re-coordination on other donor atoms, going to a weaker ligand field (from $C=O^-$ to $C=O$) associated to a switch of spin state. We have then compared the impact of HCl on C^1 with other weaker acids by UV-visible spectroscopy (Figure S15). As shown in Figure 3b the absorption spectrum of the ligand is only modified in presence of HCl, indicating that weak acids do not protonate the linkers and that if a change is observed for C^1 in presence of formic acid, it will be due to a spin state change rather to a protonation of the complex.

2.3.2. UV-Visible Absorption Studies in Solid Phase of Complex C^1 and of C^1 MOF-808 Under Vapor

To evaluate the behavior of C^1 in the solid state, a solution of the complex was drop casted and dried on a piece of glass and placed in a hermetic chamber. The influence of the optical absorption of the film in presence of saturated vapors (low concentration did not show any significant impact on the absorbance) were then measured (Figure S21), evidencing that except for HCl, where the absorption spectrum is drastically different, the other solvents led to absorption spectra with similar shapes and different relative intensities, in agreement with the fact that the vapors are inducing a slight change in spin state of C^1 , as already observed in solution.

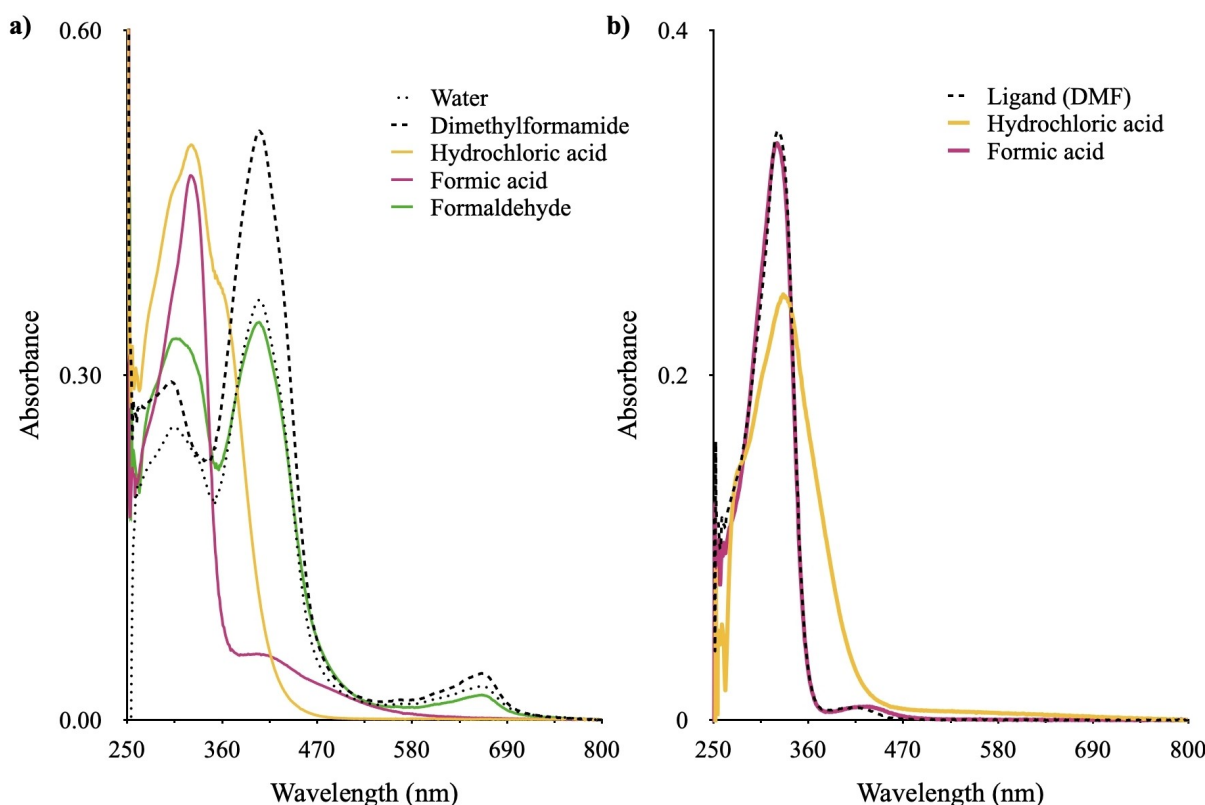


Figure 3. a) Optical absorption spectra of C^1 in different solvents; b) Optical absorption spectra of the ligand in DMF and in presence of acids.

In order to study the impact of vapors on the hybrid C^1 MOF-808 compound, the solid was first shaped via spin coating (See ESI*, Figure S17, S18) to obtain a 650 nm thick homogenous film. A series of *in situ* preliminary tests was performed (See ESI*) to determine the standard deviation on absorbance (0.0025 Figure S19) and the absorbance of MOF-808 alone (Figure S20).

The impact of water vapor sorption on the optical absorbance of the films was then studied (Figure S16). Results showed that even if MOF-808 is slightly hydrophilic,^[19] no impact of water sorption on the optical absorbance of the hybrid materials was observed, even in highly humid environment, suggesting that this compound might be used for VOCs vapor sensing in presence of water vapor (see ESI*).

A C^1 MOF-808 (Figure 4a) film prepared by spin coating was then placed under highly saturated vapor of several solvents (100 μ L of liquid placed in the chamber close to the film) to evaluate its potential for chemosensing. Unlike the complex C^1 , there was no absorbance response in most cases except for formaldehyde and formic acid (See Figure S22 for all other VOCs tested). Noteworthy, these changes were shown to be totally reversible after few minutes at room temperature once taking out of the VOCs environment (Figure S23–S24). Since the material only responds to formaldehyde and formic acid, the rest of the study was focused on those two VOCs. Their colorimetric properties are nevertheless different, going

from medium yellowish-green to pale yellow (formaldehyde) or to whitish (formic acid) (Figure 4b).

The evolution of the optical absorbance in presence of vapors (Figure S23b–S24b) is consistent with a LS to HS conversion associated to a well-defined isosbestic point at 380 nm with formic acid, while with formaldehyde, the isosbestic point is located around 430 nm and a shift of the pic at 305 nm to 315 nm is observed. The same shift can be observed with MOF-808 alone in presence of formaldehyde vapors (Figure S20b) and can be attributed to the adsorption of the VOCs in the MOF's pores.

To confirm that the color switching of C^1 MOF-808 arises from its SCO properties, infrared spectra under vapor were registered (Figure 5).^[23–26] In presence of formaldehyde vapor, three characteristics vibrational bands of the complex are shifted: the $\nu_{N=C}$ from 1602 to 1580 cm^{-1} , the δ_{C-N} from 1294 to 1271 cm^{-1} , and finally the δ_{pyridine} at 760 cm^{-1} splits with the apparition of a band at 732 cm^{-1} . The decrease in energy of vibrational bands positions can be attributed to a conversion from LS to HS induced by the vapor. For formic acid, due to the large number of vibrational bands of this acid in the 1650–1500 cm^{-1} the $\nu_{N=C}$ could not be observed. However, two major shifts can be distinguished: a first shift from 1294 to 1286 cm^{-1} , a second from 760 cm^{-1} to 738 cm^{-1} that can be attributed to a conversion from LS to HS.

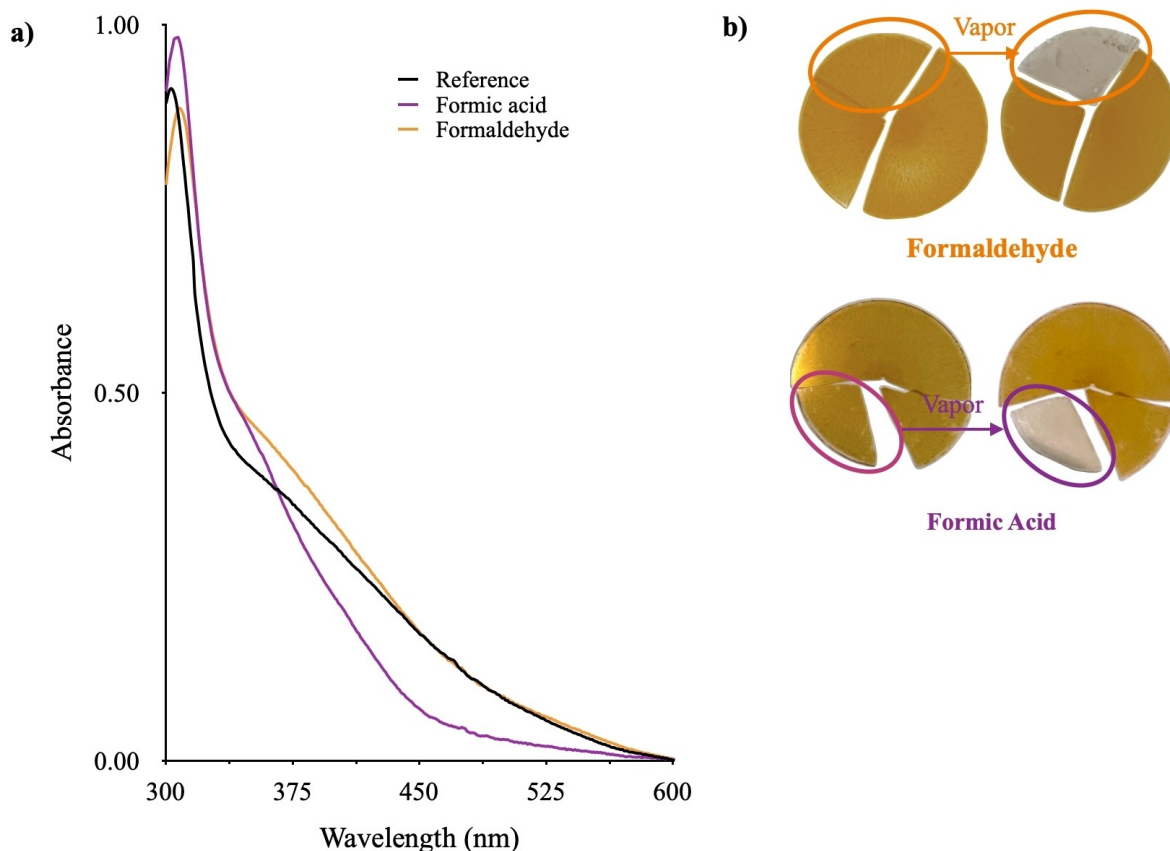


Figure 4. a) Solvent dependence of the optical absorption spectrum at 298 K of C^1 MOF-808; b) Picture of C^1 MOF-808 on glass slide exposed to high vapor pressure vapor of formaldehyde and formic acid.

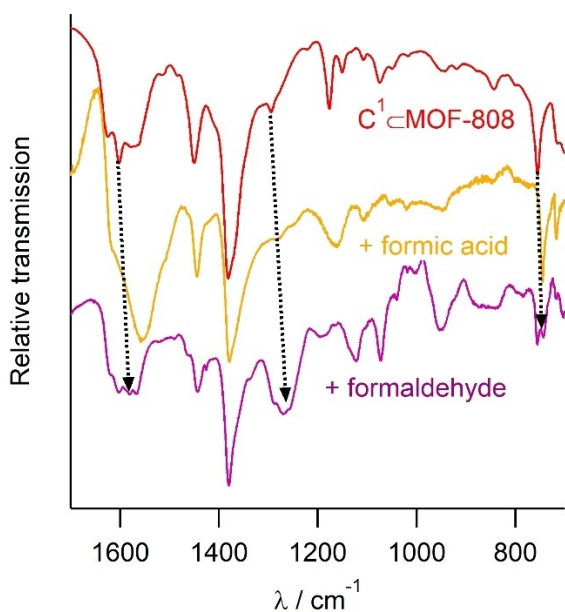


Figure 5. Comparison of Infrared spectra of C^1 -MOF-808 under formaldehyde and under formic acid vapor sorption (see ESI Figure S25a and Figure S25b for Infrared spectra of the solvent and Figure S.26 for full range spectra in presence of vapors).

2.3.3. Formaldehyde Vapor Sensing Through UV-Visible Absorption Studies

Formaldehyde is a well-known harmful indoor pollutant, of natural or anthropogenic origin, which can be found in industry, manufacture and also in medicine.^[27] This compound can cause serious health problems from chronic disease to cancer.^[28] European union delimited the exposure time of formaldehyde to 0.6 ppm for 15 minutes and to 0.3 ppm for 8 hours.^[29]

C^1 -MOF-808 films were exposed to formaldehyde vapors at different gradient of concentrations (See ESI*) to determine minimum concentration in ppm that the compound will react to. In the first experiment, the film was exposed to a highly concentrated environment to study the evolution of absorbance and the kinetics of the reaction under formaldehyde sorption (change of color in comparison with C^1 film). As seen in Figure 6, for a concentration of 120 ppm, an evolution of the optical absorbance consistent with a LS to HS conversion is observed. The kinetics of the transition was extracted following the optical absorption at 380 nm (maximum of the absorbance) and showed that the absorbance reaches a plateau after 20 minutes, with 75% of the modification that occurred before 5 minutes, indicating the fast reaction of the compound with the VOC.

A similar study was carried out with concentrations of 12, 7 and 2.8 ppm of formaldehyde (Figure S28-30), leading to similar evolution of the absorption spectrum in each case (Figure S30).

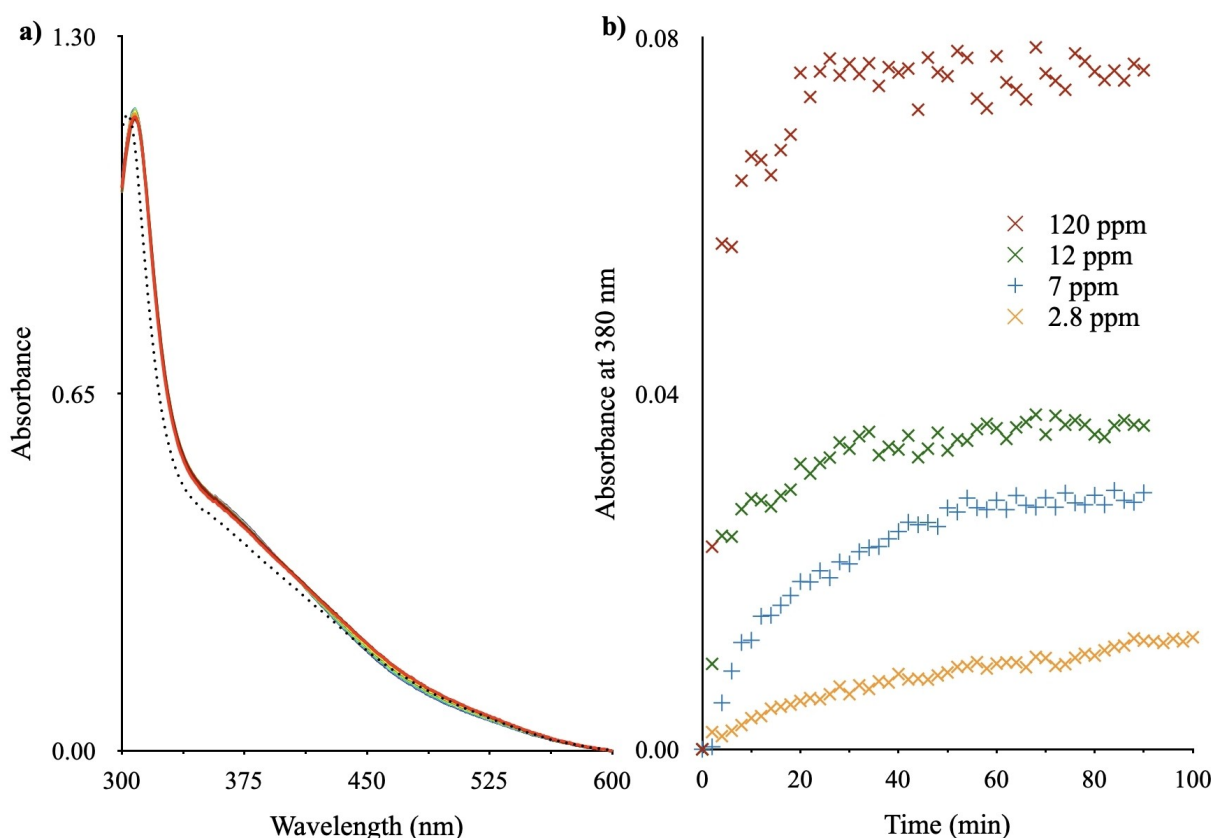


Figure 6. Evolution of the optical properties of C^1 -MOF-808 upon formaldehyde vapor: a) UV-visible spectra in presence of 120 ppm of formaldehyde as function of time (one scan/2 min); b) Kinetics of absorbance at 380 nm in presence of 120, 12, 7 and 2.8 ppm of formaldehyde.

Under a concentration of 12 ppm, the same shape of the kinetics behavior was observed, with an absolute variation of the absorbance divided by two compared to the one at 120 ppm (Figure S30b). When lowering the concentration at 7 ppm the kinetics of the absorption slowed down: 50 % of the change occurred in 30 minutes and the maximum was reached after 50 minutes. The limit concentration reached with this compound was estimated around 3 ppm. Indeed, when working with lower values of concentration, very limited modifications of the optical spectrum shape or of the absorbance value was observed. In addition, the transformation becomes really slow at such a low concentration as the equilibrium state was not reached after 100 minutes of exposure, which can be due to the diffusion kinetics of formaldehyde inside the pores and/or to the competition with the sorption of nitrogen that is in large excess in the carrier gas.

To confirm that a color change can be observed with naked eye, a piece of film was inserted inside a jar a filled with 2.8 ppm of formaldehyde. As seen on Figure 7a, a switch from dark green to lighter was observed confirming the sensitivity of the device (See Figure S31). Then, the PXRD pattern (Figure S27) of the retrieved treated compound with formaldehyde was collected and no changes were observed, indicating the preservation of the hybrid material structure.

2.3.4. Formic Acid Vapor Sensing Through UV-Visible Absorption Studies

Formic acid, like formaldehyde, can be found in a numerous industry (building, food, ...).^[30] Even if no direct health problem is reported for it for low concentration, it was shown that a high vapor concentration, this highly polar VOC can be metabolized into methanol that can harm the human system.^[31] At higher concentration, it is known to be harmful for the respiratory system^[32] and therefore, European union classified formic acid as a dangerous VOC with an exposure limit 5 ppm.^[33] Moreover, formic acid is known to be involved in the degradation of cellulose and its monitoring is therefore of importance for cultural heritage preservation.^[12]

The evolution of the optical absorbance of C¹C-MOF-808 as function of the time under various concentrations of formic acid was registered (Figure S32-34). For high concentration (720 ppm), the kinetics of the transformation was really fast with a significant change in the absorbance (around 0.045) monitored from the band at 370 nm: in one minute 50 % of the conversion was already observed and after 3 minutes, more than 90 % was reached (See Figure 8).

When lowering the concentration from 710 ppm to 94 ppm, no drastic changes are observed (Figure 8b). However, as the concentration decreased to 45 ppm of formic acid, (Figure S32c-S34c) the kinetics starts to slow down and the transformation become less quantitative, with an evolution of the absorbance at 370 nm going from 0.045 at 710 ppm to 0.028 at 45 ppm.

By decreasing the concentration to 14 ppm (generated from a formic acid solution at 0.1 M in water) a change in the absorbance is still observed (Figure S32d, S34d) but the kinetics drastically slows down and the plateau was reached after more than 20 minutes. This value corresponds to the limit of detection for formic acid, as concentrations lower than 14 ppm didn't induce any change in the absorbance. One possible reason for this limitation is that the formic acid vapors are generated from a water solution, which may lead to a competition between the sorption of formic acid and of water inside the pores of the MOF (at 200 ml/min, the carrier gas contains around 3000 ppm of water). The same phenomenon may also affect the formaldehyde sensing at high concentration, where the vapors were generated from a formaldehyde solution in water (30 % stabilized with methanol).

As done with formaldehyde, in Figure 8b a piece of the compound was inserted in a flask filled with 14 ppm of formic acid and after one hour, a color change from kaki-yellow to almost colorless was observed (Figure S35). This color change was reversible once the piece of glass was taken out of the jar, and a PXRD pattern of the compound was then collected (Figure S27), evidencing that the treatment with formic acid did not induce any change in the MOF structure.

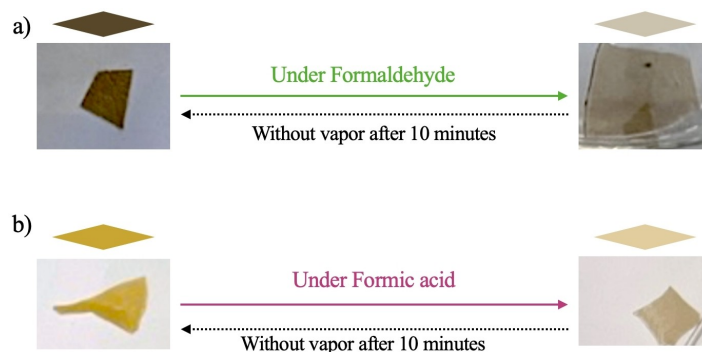


Figure 7. One hour exposing time in a flask containing piece of hybrid material on glass filed with a) 2.8 ppm of formaldehyde (concentration checked using passive dosiube from Gastec 0.5-20 ppm range); b) 14 ppm of formic acid (concentration checked using passive dosiube from Gastec 0.5-100 ppm range with a correcting factor).

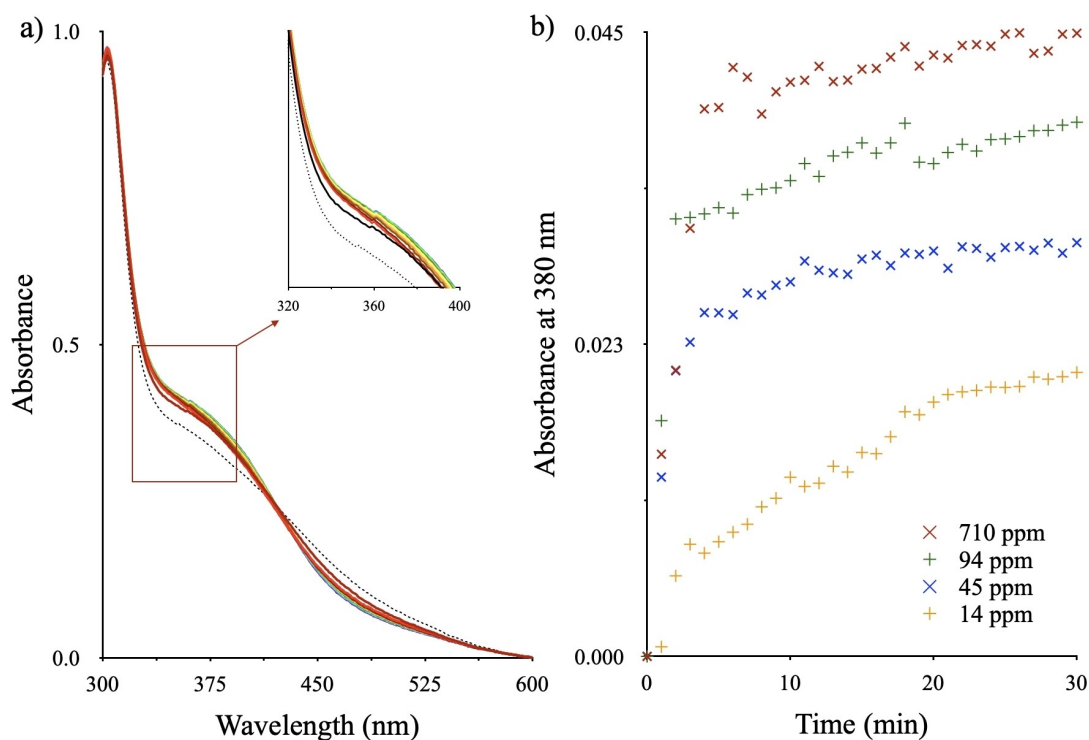


Figure 8. Evolution of the optical properties of C^1 -MOF-808 film upon formic acid vapor sorption: a) UV-visible spectra in presence of 710 ppm of formic acid as function of time (one scan/1 min); b) Kinetics of absorbance at 370 nm for concentrations of 710, 94, 45 and 14 ppm of formic acid.

2.3.5. Discussion

The C^1 -MOF-808 hybrid material appears to be sensitive as well as somewhat selective to formic acid and formaldehyde in comparison to other VOCs tested. This selectivity is not likely coming from the MOF itself, as other polar vapors can be easily adsorbed in MOF-808 without causing any change of the electronic state of the C^1 complexes loaded in the pores. Therefore, we can hypothesize that the switching originates from interactions between the adsorbed VOC molecules, the C^1 complexes and the MOF backbone. Indeed, we recently evidenced that the host-guest interactions between an Fe(III) SCO complex and MOF-808(Zr) were at the origin of the switching properties of the host complexes^[19]. Formic acid and formaldehyde possess a quite similar chemical formula and structure and their sorption in Zr(IV) carboxylate based MOFs have been already investigated, evidencing preferential sorption sites, either on the Lewis acid sites of Zr(IV) and/or on Brønsted basic groups on the linkers (for example $-NH_2$ groups)^[34]. Similarly, the two VOCs vapors are likely to interact with the Brønsted basic sites ($-NH$ groups) of SCO complexes loaded in the MOF pore. Therefore, we hypothesize that the sorption of formaldehyde or formic acid in the pores of C^1 -MOF-808 modifies the supramolecular interactions between the SCO complexes and the MOF, which consequently leads to the stabilization of the HS state of the complexes. These results evidence that controlling the intermolecular interactions between the MOF, the SCO complex and the VOC molecules is a

promising strategy to prepare hybrid films for reversible colorimetric sensing.

3. Conclusions

We report here the synthesis and characterization of a new hybrid material combining spin crossover complex and the large pore diamagnetic Zr-MOF MOF-808. When the SCO complex is incorporated inside the pores of MOF-808, the MOF retains its crystallinity, its shape and keeps a partial porosity. The SCO complex also retains its structure when encapsulated, but does not longer present a thermal spin transition and stays in a mixed spin state. We then showed that such hybrid structure could nevertheless be applied to detect precisely and sensitively VOCs compound like formic acid and formaldehyde close to the official LoD determined by governments. Moreover, these changes can be seen by a naked eye and are totally reversible even after exposure to high concentrations of VOCs. Therefore, this new class of compounds can be seen as an advanced type of material that once tuned properly, might be used for developing new colorimetric and reversible sensing devices target to a specific VOC. Even if these materials look promising, the use of large pores more hydrophobic MOFs could be an alternative to lower the minimum concentration detectable, since the hydrophilic MOF-808 captures water fairly easily. In addition, using specific MOFs with ultra-high selective vapor sorption properties^[12] and tuning how the SCO complexes interact with it are other relevant strategies to further

enhance the sensitivity and the selectivity of this kind of sensor. Finally, one would need to investigate the switching properties of these films in complex mixtures of VOCs and possibly to use them using a multiplexing approach to go towards real sensing devices.

4. Associated Content

Detail of synthetic protocols, additional characterization of solids, liquids, and methodology study can be found in the ESI Supporting Information.

Author Contributions

E.C. performed all chemical/analytical syntheses and wrote the manuscript supervised by A.T.; G.P. performed TEM analyses. All authors have given approval to the final version of the manuscript.

Acknowledgements

A.T. and E.C. thanks the ANR MOFSCO (ANR-18-CE09-0005-01) for funding the project. This work was done within the C2N micro nanotechnologies platforms and partly supported by the RENATECH network and the DIM Respire from the Ile-de-France region.

Conflict of Interests

The authors declare no conflict of interest.

Data Availability Statement

The data that support the findings of this study are available from the corresponding author upon reasonable request.

- [1] a) J. D. Spengler, *Science* **1983**, *4605*, 9–17; b) A. P. Jones, *Atmos. Environ.* **1999**, *33* (28), 4535–4564; c) P. Wolkoff, *Int. J. Hyg. Environ. Health* **2018**, *221* (3), 376–390.
- [2] a) *Industrial Emissions Directive* (Directive 2010/75/EU of the European Parliament and of the Council of 24 November **2010**); b) World Health Organization. Occupational and Environmental Health Team, **2000**: Guidelines for air quality (WHO/SDE/OEH/00.02-190).
- [3] a) D. A. Sarigiannis, S. P. Karakitsios, A. Gotti, I. L. Liakos, A. Katsoyiannis, *Environ. Int.* **2011**, *37* (4), 743–765; b) X. Yue, N. L. Ma, C. Sonne, R. Guan, S. S. Lam, Q. Van Le, X. Chen, Y. Yang, H. Gu, J. Rinklebe, W. Peng, *J. Hazard. Mater.* **2021**, *405*, 124138; c) C. He, J. Cheng, X. Zhang, M. Douthwaite, S. Pattison, Z. Hao, *Chem. Rev.* **2019**, *119*, 4471–4568.
- [4] a) M. R. Ras, F. Borrull, R. M. Marcé, *TrAC Trends Anal. Chem.* **2009**, *28* (3), 347–361; b) B. Szulczyński, J. Gębicki, *Environments* **2017**, *4* (1), 21.
- [5] a) M. A. Halcrow, *Spin-Crossover Materials: Properties and Applications*, John Wiley & Sons Ltd, **2013**, Chapter I–III; b) P. Gütllich, H. A. Goodwin, *Top. Curr. Chem.* **2004**, 233.
- [6] a) P. Gütllich, A. Hauser, H. Spiering, *Angew. Chem. Int. Ed.* **1994**, *33* (20), 2024–2054; b) J.-F. Létard, *Mater. Chem.* **2006**, *16*, 2550–2559; c) O. Sato, J. Tao, Y.-Z. Zhang, *Angew. Chem. Int. Ed.* **2007**, *46*, 2152–2187.
- [7] a) P. Gütllich, A. B. Gaspar, Y. Garcia, *Beilstein J. Org. Chem.* **2013**, *9*, 342–391; b) M. M. Khusniyarov, *Chem. Eur. J.* **2016**, *22* (43), 15178–15191.
- [8] M. Ohba, K. Yoneda, G. Agusti, M. C. Munoz, A. B. Gaspar, J. A. Real, M. Yamasaki, H. Ando, Y. Nakao, S. Sakaki, S. Kitagawa, *Angew. Chem.* **2009**, *121*, 4861–4865.
- [9] a) H. M. Powell, J. H. Rayner, *Nature* **1949**, *163* (4145), 566–567; b) T. Kitazawa, Y. Gomi, M. Takahashi, M. Takeda, M. Enomoto, A. Miyazaki, T. Enoki, *J. Mater. Chem.* **1996**, *6*, 119–121; c) C. Bartial-Murgui, A. Akou, H. J. Shepherd, G. Molnar, J. A. Real, L. Salmon, A. Bousseksou, *Chem. Eur. J.* **2013**, *19*, 15036–15043; d) G. Agusti, R. Ohtani, K. Yoneda, A. B. Gaspar, M. Ohba, J. F. Sanchez-Royo, M. C. Munoz, S. Kitagawa, J. A. Real, *Angew. Chem. Int. Ed.* **2009**, *48*, 8944–8947; e) R. Ohtani, K. Yoneda, S. Furukawa, N. Horike, S. Kitagawa, A. B. Gaspar, M. C. Munoz, J. A. Real, M. Oba, *J. Am. Chem. Soc.* **2011**, *133*, 8600–8605; f) T. Kosone, T. Kitazawa, *Inorg. Chem. Acta* **2016**, *439*, 159–163; g) Z.-P. Ni, J.-L. Liu, M. N. Hoque, W. Liu, J.-Y. Li, Y.-C. Chen, M.-L. Tong, *Coord. Chem. Rev.* **2017**, *335*, 28–43.
- [10] O. M. Yaghi, M. O’Keeffe, N. W. Ockwig, H. K. Chae, M. Eddaoudi, J. Kim, *Nature* **2003**, *423* (6941), 705–714.
- [11] G. Maurin, C. Serre, A. Cooper, G. Férey, *Chem. Soc. Rev.* **2017**, *46*, 3104–3107.
- [12] a) L. E. Kreno, K. Leong, O. K. Farha, M. Allendorf, R. P. Van Duyne, J. T. Hupp, *Chem. Rev.* **2012**, *112*, 1105–1125; b) Z. Hu, B. J. Deibert, J. Li, *Chem. Soc. Rev.* **2014**, *43*, 5815–5840; c) P. Mü, F. M. Wisser, P. Freund, V. Bon, I. Senkovska, S. Kaskel, *Inorg. Chem.* **2017**, *56* (22), 14164–14169; d) Y. Shen, A. Tissot, C. Serre, *Chem. Sci.* **2022**, *46* (13), 13978–14007; e) M. I. Severino, A. Al Mohtar, C. Vieira Soares, O. Kolmykoc, C. Freitas, I. Dovgaliuk, C. Martineau, V. Pimenta, F. Nouar, G. Maurin, M. L. Pinto, C. Serre, *J. Mater. Chem. A* **2023**, *11*, 4238–4247; f) M. I. Severino, A. Al Mohtar, C. Vieira Soares, N. Sadovnik, C. Freitas, S. Nandi, G. Mouchaham, V. Pimenta, F. Nouar, M. Daturi, G. Maurin, M. L. Pinto, C. Serre, *Angew. Chem. Int. Ed.* **2023**, *62*, e202211583.
- [13] J. He, J. Xu, J. Yin, N. Li, X.-H. Bu, *Sci. China Mater.* **2019**, *62*, 1655–1678.
- [14] X. Y. Liu, X. M. Yin, S. L. Yang, L. Zhang, R. Bu, E. Q. Gao, *ACS Appl. Mater. Interfaces* **2021**, *13* (17), 20380–20387.
- [15] T. Zhao, I. Boldog, V. Spasojevic, A. Rotatu, Y. Garcia, C. Janiak, *J. Mater. Chem. C* **2016**, *4*, 6588–6601.
- [16] F. Moreau, J. Marrot, F. Banse, C. Serre, A. Tissot, *J. Mater. Chem. C* **2020**, *8*, 16826–16833.
- [17] A. Tissot, X. Kesse, S. Giannopoulou, I. Stenger, L. Binet, E. Rivère, C. Serre, *Chem. Commun.* **2019**, *55* (2), 194–197.
- [18] Y. Shen, J. Woodburn, S. Bouras, S. Dai, I. Dovgaliuk, J.-M. Grenèche, G. Patriarche, L. M. Lawson Daku, C. Serre, A. Tissot, *Chem. Mater.* **2023**, *35* (2), 719–727.
- [19] H. Furukawa, F. Gándara, Y.-B. Zhang, J. Jiang, W. L. Queen, M. R. Hudson, O. Yaghi, *J. Am. Chem. Soc.* **2014**, *136* (11), 4369–4381.
- [20] S. Dai, C. Simms, I. Dovgaliuk, G. Patriarche, A. Tissot, T. N. Parac-Vogt, C. Serre, *Chem. Mater.* **2021**, *33*, 7057–7066.
- [21] X.-Q. Chen, Y.-D. Cai, W. Jiang, G. Peng, J.-K. Fang, J.-L. Liu, M.-L. Tong, X. Bao, *Inorg. Chem.* **2019**, *58*, 999–1002.
- [22] D. K. Johnson, T. B. Murphy, N. J. Rose, W. H. Goodwin, L. Pickart, *Inorg. Chim. Acta* **1982**, *67*, 159–165.
- [23] K. Nakamoto, *Infrared and Raman Spectra of Inorganic and Coordination Compounds – Part B: Applications in Coordination, Organometallic, and Bioinorganic Chemistry*, Wiley, **2015**.
- [24] M. Sorai, S. Seki, *J. Phys. Chem. Solids* **1974**, *35* (4), 555–570.
- [25] G. Brehm, M. Reiher, B. Le Guennic, M. Leipold, S. Schindler, F. W. Heinemann, *J. Raman Spectrosc.* **2006**, *37*, 108–122.
- [26] P. Durand, S. Pillet, E.-E. Bendelf, C. Carteret, M. Bouazaoui, H. El Hamzaoui, B. Capoen, L. Salmon, S. Hébert, J. Ghanbaja, L. Aranda, D. Schaniel, *J. Mater. Chem. C* **2013**, *1*, 1933–1942.
- [27] a) Y. Liu, H. Yang, C. Ma, S. Luo, M. Xu, Z. Wu, W. Li, S. Liu, Y. Liu, C. Ma, S. Luo, M. Xu, Z. Wu, W. Li, S. Liu, *ACS Appl. Mater. Interfaces* **2020**, *12*, 36628–36638; b) T. Salthammer, S. Mentese, R. Marutzky, *Chem. Rev.* **2010**, *110*, 2536–2572; c) A. H. Khoshakhlagh, K. J. Chuang, P. Kumar, *Environ. Sci. Pollut. Res. Int.* **2023**, *30*, 16386–16397.
- [28] a) J. Ye, Y. Yu, J. Fan, B. Cheng, J. Yu, W. Ho, *Environ. Sci.: Nano* **2020**, *7*, 3655–3709; b) N. Soonklang, S. Saowakon, *Environ. Sci. Pollut. Res. Int.* **2022**, *29*, 65642–65654; c) D. A. Sarigiannis, S. P. Karakitsios, A. Gotti, I. L. Liakos, A. Katsoyiannis, *Environ. Int.* **2011**, *37* (4), 743–765.
- [29] European Union Official journal: DIRECTIVE (UE) 2019/983/L 164/23.
- [30] N. Suzuki, H. Nakaoka, A. Eguchi, M. Hanazato, Y. Nakayama, K. Tsumura, K. Takaguchi, K. Takaya, E. Todaka, C. Mori, *Int. J. Environ. Res. Public Health* **2020**, *17* (6), 1940–1950.
- [31] J. Liesivuori, H. Savolainen, *Pharmacol. Toxicol.* **1991**, *69* (3), 157–163.

- [32] D. T. Watts, *Arch. Biochem. Biophys.* **1951**, *34* (2), 391–395.
- [33] European Union Official journal: DIRECTIVE 2006/15/CE/L 38/36.
- [34] a) K. Dedecker, R. S. Pillai, F. Nouar, J. Pires, N. Steunou, E. Dumas, G. Maurin, C. Serre, M. L. Pinto, *ACS Appl. Mater. Interfaces* **2018**, *10*, 13886–13894; b) K. Vellingiri, Y.-X. Deng, K.-H. Kim, J.-J. Jiang, T. Kim, J. Shang, W.-S. Aha, D. Kukkar, D. W. Boukhvalov, *ACS Appl. Mater. Interfaces* **2019**, *11*, 1426–1439; c) K. Vikrant, Y.-X. Deng, K.-H. Kim, S. A. Younis, D. W. Boukhvalov, W.-S. Ahn, A. Deep, *ACS Appl. Mater. Interfaces* **2019**, *11*, 44270–44281; d) K. Vikrant, Y. Qu, J. E. Szulejko, V. Kumar, K. Vellingiri,

D. W. Boukhvalov, T. Kim, K.-H. Kim, *Nanoscale* **2020**, *12*, 8330–8343;
e) T. Y. Tran, S. A. Younis, P. Heynderickx, K.-H. Kim, *J. Hazard. Mater.* **2022**, *424B*, 127459–127471.

Manuscript received: February 1, 2024
Accepted manuscript online: May 3, 2024
Version of record online: June 20, 2024